

Original Article

Invivo and invitro evaluation of antitumor effects of iron oxide and folate core shell-iron oxide nanoparticles

Avaliação in vivo e in vitro dos efeitos antitumorais de nanopartículas de óxido de ferro e óxido de ferro com núcleo de folato

N. N. H. Shosha^{a*} , S. Elmasry^a , M. Moawad^b , S. H. Ismail^c  and M. Elsayed^a 

^aAin Shams University, Faculty of women for Arts Science and Education, Department of Biochemistry and Nutrition, Cairo, Egypt

^bCairo University, National Cancer Institute, Pathology Department, Cairo, Egypt

^cCairo University, Egypt Nanotechnology Center, Giza, Egypt

Abstract

Nanoparticles are considered viable options in the treatment of cancer. This study was conducted to investigate the effect of magnetite nanoparticles (MNPs) and magnetite folate core shell (MFCS) on leukemic and hepatocarcinoma cell cultures as well as their effect on the animal model of acute myelocytic leukemia (AML). Through current study nanoparticles were synthesized, characterized by various techniques, and their properties were studied to confirm their nanostructure. Invivo study, nanoparticles were evaluated to inspect their cytotoxic activity against SNU-182 (human hepatocellular carcinoma), K562 (human leukemia), and THLE2 (human normal epithelial liver) cells via MTT test. Apoptotic signaling proteins Bcl-2 and Caspase-3 expression were inspected through RT-PCR method. A cytotoxic effect of MNPs and MFCS was detected in previous cell cultures. Moreover, the apoptosis was identified through significant up-regulation of caspase-3, with Bcl-2 down-regulation. Invitro study, AML was induced in rats by N-methyl-N-nitrosourea followed by oral treatment with MNPs and MFCS. Biochemical indices such as aspartate and alanine amino transferases, and lactate dehydrogenase activities, uric acid, complete blood count, and Beta -2-microglobulin were assessed in serum. Immunophenotyping for CD34 and CD38 detection was performed. Liver, kidney, and bone marrow were microscopically examined. Bcl-2 promoter methylation, and mRNA levels were examined. Although, both MNPs and MFCS depict amelioration in biochemical parameters, MFCS alleviated them toward normal control. Anticancer activity of MNPs and MFCS was approved especially for AML. Whenever, administration of MFCS was more effective than MNPs. The present work is one of few studies used MFCS as anticancer agent.

Keywords: cancer, leukemia, folate, iron oxide, nanoparticles.

Resumo

Nanopartículas são consideradas opções viáveis no tratamento do câncer. Este estudo foi conduzido para investigar o efeito de nanopartículas de magnetita (MNPs) e núcleo de folato de magnetita (MFCS) em culturas de células leucêmicas e de hepatocarcinoma, bem como seu efeito no modelo animal de leucemia mielocítica aguda (LMA). Através do atual estudo, nanopartículas foram sintetizadas, caracterizadas por várias técnicas, e suas propriedades foram estudadas para confirmar sua nanoestrutura. No estudo in vivo, as nanopartículas foram avaliadas para inspecionar sua atividade citotóxica contra células SNU-182 (carcinoma hepatocelular humano), K562 (leucemia humana) e THLE2 (fígado epitelial humano normal) por meio do teste MTT. A expressão das proteínas sinalizadoras apoptóticas Bcl-2 e Caspase-3 foram inspecionadas através do método RT-PCR. Um efeito citotóxico de MNPs e MFCS foi detectado em culturas de células anteriores. Além disso, a apoptose foi identificada por meio de regulação positiva significativa da Caspase-3, com regulação negativa de Bcl-2. No estudo in vitro, a AML foi induzida em ratos por N-metil-N-nitrosourea seguida por tratamento oral com MNPs e MFCS. Índices bioquímicos como aspartato e alanina aminotransferases e atividades de lactato desidrogenase, ácido úrico, hemograma completo e Beta-2-microglobulina foram avaliados no soro. A imunofenotipagem para detecção de CD34 e CD38 foi realizada. Fígado, rim e medula óssea foram examinados microscopicamente. A metilação do promotor Bcl-2 e os níveis de mRNA foram examinados. Embora tanto os MNPs quanto os MFCS representem uma melhora nos parâmetros bioquímicos, o MFCS os aliviou em direção ao controle normal. A atividade anticâncer de MNPs e MFCS foi aprovada especialmente para AML. Sempre, a administração de MFCS foi mais eficaz do que MNPs. O presente trabalho é um dos poucos estudos que utilizou o MFCS como agente anticâncer.

Palavras-chave: câncer, leucemia, folato, óxido de ferro, nanopartículas.

*e-mail: Nehad.shosha@women.asu.edu.eg

Received: June 11, 2021 – Accepted: October 1, 2021



This is an Open Access article distributed under the terms of the Creative Commons Attribution License, which permits unrestricted use, distribution, and reproduction in any medium, provided the original work is properly cited.

1. Introduction

Cancer is a group of diseases involving abnormal cell growth with the potential to invade or spread to other parts of the body (Kumari, 2020). Leukemia is blood cancer related to white blood cells. It arises when abnormal white blood cell begins to continuously replicate itself and not function normally. As they accumulate, they inhibit the production of other normal blood cells in the marrow, leading to anemia, bleeding, and recurrent infections. Over time, the leukemic cells spread through the bloodstream where they continue to divide, sometimes forming tumors and damaging organs such as the kidney and liver. Acute leukemia is classified into two types: Acute Lymphoblastic Leukemia (ALL) and Acute Myeloid Leukemia (AML). Acute leukemia is a rapidly progressing disease that affects mostly cells that aren't yet fully developed or differentiated). ALL is most common in children while AML mainly affects adults but can occur in children and adolescents (Joshi et al., 2013).

Acute myeloid leukemia (AML) represents a group of clonal hematopoietic stem cells failed to differentiate into mature cells and excessive proliferation in the bone marrow stem cell compartment result in the accumulation of myeloblasts (Hill and Sekeres, 2009). AML comprises a heterogeneous group of neoplastic disorders in which $\geq 20\%$ of bone marrow cells are myoblasts (Hwang, 2020). The CD34+/CD38- immunophenotype is used to identify hematopoietic stem cells and leukemia-initiating cells in AML (Jiang et al., 2016).

The cause of leukemia is poorly understood in most cases, but it appears to involve some rearrangement of DNA. Leukemia develops in animals, either spontaneously or because of treatment with external or internal leukemogenic factors. External factors include alkylating drugs, ionizing radiation, or chemicals. Internal factors include chromosomal abnormalities leading to DNA changes. N-methyl-N-nitrosourea (NMU) is a nitrosourea compound with alkylating property and a highly potent direct-acting carcinogen that is capable of inducing tumor formation. NMU induced specifically acute myelocytic leukemia (AML) in Sprague–Dawley rats (Chang et al., 2012).

The development of nanoparticles (NPs) for use in all facets of oncological disease detection and therapy has shown great progress over the past two decades (Revia and Zhang, 2016). Magnetic nanoparticles (MNPs) have gained immense attention for cancer theragnostic applications due to their unique physicochemical properties, magnetic resonance imaging (MRI) contrast, facile synthesis, easy surface decorations, low toxicity, and good biodegradability that assist them to serve as outstanding imaging agents, and delivery vehicles in cancer therapy (Mukherjee et al., 2020).

Targeted delivery system is a promising strategy for improving cancer treatment and diagnostics (Tyagi et al., 2016). Folic acid (FA) has a high affinity for folate receptors (FRs), which are over-expressed in various types of human tumors including blood carcinomas but are generally absent in most normal tissues. Therefore, FA is an effective and non-immunogenic target ligand for cancer cells (Shen et al., 2015).

This provides tumor cells with increased amounts of the FA, which is essential for DNA synthesis and seems

to aid in aggressive tumor growth. In patients with blood cancer, the overexpression of FR isoform correlates with a higher histological grade and a more advanced stage of the disease. The differential expression of FR in blood and other cancers makes it an attractive marker and target molecule for diagnosis and therapy of the disease (Low et al., 2008). Also, Folate metabolites serve as a cofactor for numerous methylation reactions of DNA, Alterations in DNA methylation density also influence gene expression. Tumor suppressor genes seem to be particularly sensitive to methylation silencing tumor progression (Tyagi et al., 2016).

Treatment of cancer using nanoparticles made of inorganic and metallic compounds has been increasingly used, owing to their novel intrinsic physical properties and their potential to interact with specific cellular sites, thereby significantly reducing severe secondary effects. Recently, many studies have used folic acid on nanocarriers for the specific targeting of over-expressing FRs on cancer cells (Mondal et al., 2019), but information on using folic acid as a core shell of magnetite iron oxide nanoparticles (MNPs) and exploration of its cytotoxic effect have not yet been reported. The present study was designed to assess the effect of both (MNPs) and their folate core shell structure (MFCS) nanoparticles on different cancer cells culture and then, investigate their effect on AML model induced in rats.

2. Materials and Methods

2.1. Preparation of magnetite iron oxide and folate core shell iron oxide Nanoparticles:

2.1.1. Synthesis of magnetite nanoparticles (MNPs)

Magnetite as nano-mineral was synthesized by co-precipitation method with ammonia as a reducing agent and polyethylene glycol (PEG) 600 as a stabilizer (Ismail et al., 2020). In a typical synthesis, $\text{FeCl}_3 \cdot 6\text{H}_2\text{O}$ solution (0.6 M) was mixed with 0.3M FeCl_2 solution and the mixture was heated with constant stirring at 55 °C for 20 min until a dark orange solution was formed. Then, ammonia was added drop by drop until all solution became black. Ammonia drops continued until the pH of the mixture equal 12. Serious washing had been done using deionized water, methanol, and external magnets several times until pH almost equal 7 then the wet precipitate left to air dry for 24 hours, then 2 ml of PEG 600 were added and the mixture was subjected to stirring by a mechanical stirrer for 2 hours.

2.1.2. Synthesis of magnetite – folic core-shell nanostructure (MFCS)

Folic acid of 0.1 g was added to 100 ml deionized water and stirred for 30 min, at 60 °C then subjected to ultrasonication under condition of 0.9 cycle and 90% amplitude for 2 hours. 0.1 g of magnetite nanoparticles was added to 50 ml of doubled deionized water and stirred for 0.5 hours by mechanical stirrer then 50 ml of folic acid

that was previously prepared was added and the mixture was subjected to sonication for 6 hours (0.6 cycles and 50% amplitude).

2.2. Characterization of nanoparticles

Examination of nanoparticles morphology was carried out by Transmission Electronic Microscopy (TEM) (model EM-2100 High-Resolution- Japan) at magnification 20X and voltage 200 kV. TEM has been done to confirm 2D shape and size. Scanning Electronic Microscope (SEM) was carried out by Jo1 2000, Japan to confirm the 3D shape and Atomic force microscope (AFM) (5600LS Agilent Technology Company) to confirm 2D and 3D roughness profile and particles. preparation of sample before measurement on AFM was done by adding sample in the form of powder in water and sonication for 5 minutes, suspension added on mica slide, at the condition of measurement (size 500 X 500 nm, speed 0.2 inch/sec, I Gain = 0.22 and P Gain = 22 using contact mode). Identification of nanoparticles was confirmed by X-ray diffraction (XRD) (D8 Discovery – Bruker Company) by using thin film carried out by spin coated instrument, condition of measurement was 40 KV and 40 AM (1600W) at speed scan 0.015 and 2theta range from 20° to 80°. Indexing of nanoparticles had been done to determine specific surface area by Branuar -Emmett – Teller (BET) method (degassing was done to remove moisture content and dust at 60 °c under vacuum (10³ c/min for 1 hour then soaking for 0.5 hour), pore size by Dubinin-Astakhov (DA) method using surface area and pore size analyzer model of Nova Touch LX2 manufacture by Quantachrome Company.

2.3. *In vitro* study

2.3.1. *In vitro* cytotoxicity assay

SNU-182 (human hepatocellular carcinoma), K562 (human leukemia cell), and THLE2 (human normal epithelial liver cell) cell cultures were used for evaluating the cytotoxicity of MNPs and MFCS against thalidomide reagent. Cell lines obtained from American Type Culture Collection were cultured using Dulbecco's modified Eagle medium DMEM (Invitrogen/Life Technologies) supplemented with 10% fetal bovine serum (FBS) (Hyclone), 10 ug/ml of insulin, and 1% penicillin-streptomycin. All the chemicals and reagents were purchased from Sigma company. Cytotoxicity assay was based on metabolic cell viability, using tetrazolium reduction assay (MTT) according to (MTT, Sigma Chemical Co.) After treatment with either one of the NPs or thalidomide, the survival of viable cells in monolayer culture was determined.

The cell's layer was rinsed with 0.25% (w/v) Trypsin 0.53 mM EDTA solution to remove all traces of serum that contains Trypsin inhibitor. 2.0 ml of Trypsin EDTA solution were added to the flask and the cells were observed under an inverted microscope until the cell layer was dispersed. 6.0 ml of complete growth medium were added, and the cells were aspirated by gently pipetting. The cell suspension was transferred to the centrifuge tube with the medium and cells were centrifuged at approximately 125 xg for 5 to 10 min. The supernatant was discarded, and the cell pellets

were resuspended in a fresh growth medium. Aliquots of the cell suspension were added to new culture vessels.

Cultures were incubated at 37°C for 24 hrs. Cells were treated with the serial concentrations (100ug/ml; 25ug/ml; 6.25ug/ml; 1.56ug/ml and 0.39ug/ml) of both NPs and thalidomide then incubated for 48 h at 37°C. The plates were examined under the inverted microscope and proceed with the MTT assay.

2.3.1.1. Determination of IC50

MTT assay test is based on the ability of living cells to reduce tetrazole (yellow) to formazan (purple) with the mitochondrial reductase; cell survival rates are calculated based on the absorbance of the formazan formed. Reconstituted MTT was added in an amount equal to 10% of the culture medium volume. Cultures were incubated for 2-4 hours depending on cell type and maximum cell density. After the incubation period, cultures were removed from the incubator and the resulting formazan crystals were dissolved by adding an amount of MTT solubilization solution [M-8910] equal to the original culture medium volume and mixed gently in a gyratory shaker to enhance dissolution. Absorbance was measured spectrophotometrically at 570 nm. The background absorbance of multi-well plates was measured at 690 nm and subtracted from the 450 nm measurement.

2.3.2. Quantitative assessment of the mRNA expression levels of *Bcl-2* and *caspase-3*

SNU-182, K562, and THLE2 cell cultures were incubated with MNPs and MFCS and the cells were collected, total RNA was extracted by the Qiagen RNA extraction kit (Qiagen Inc., Valencia, CA, USA), and reverse transcription quantitative-PCR was performed using BioRad sybergreen PCR MMX kit according to kit instructions. Beta Actin (β -ACT) expression level was used as a reference gene. Calculations were performed using the Sequence Detection system, Rotor-Gene 1.7.87 computer software.

Real-time PCR reactions were performed using the qPCR Core kit for SYBR® Green I (Eurogentec, Belgium) following the manufacturer's specifications. Typically, reaction mixtures contained 3.5 mM MgCl₂, 200 μ M each dNTP, 300 nM of each primer, 0.025 U/ μ l of HotGoldStar enzyme, 0.6 μ l of diluted SYBR® Green I, and reaction buffer in a final volume of 20 μ L. The PCR program used for amplification was: 10 min at 95 °C, 40 cycles with 15 s at 95 °C, and 1 min at 60 °C. Reactions were performed in 96-well plates with optical caps (Applied Biosystems) in a GeneAmp® 5700 Sequence Detector System (Applied Biosystems). Each sample was assayed in triplicate and analyzed with the GeneAmp® 5700 SDS v1.1 software and Microsoft Excel.

Primers for the reference and target genes were designed using the program PrimerExpress™ v1.5 and the bioinformatic tool Oligonucleotide Properties Calculator. temperature, GC content, secondary structure, and length were taken into consideration for primer design. The cDNA transcript sequences were obtained in Genbank database from NCB. The primer sequences used in this work to

amplify the Bcl-2; caspase-3 and β -actin transcripts are displayed in Table 1.

2.4. *In vivo* study

2.4.1. *Animal trail*

2.4.1.1. *Experimental animals*

The present study was carried out on 40 adult male albino rats " Sprague Dawley " obtained from Vaccine and Immunity Organization, Helwan farm, Cairo, Egypt. All experiments were conducted in accordance with the guidelines for maintenance, treatment, and killing of experimental animals. Animals were housed in stainless cages and provided a commercial diet and water *ad-libitum*. All rats were acclimatized under standard laboratory conditions for one week.

2.4.1.2. *Induction of acute myeloid leukemia (AML)*

Thirty rats were given a series of six i.v. injection of 35 mg/kg of body weight, N- methyl- nitroso-urea (NMU), at biweekly intervals (Chang et al., 2012). NMU was injected in a caudal vein; the day of the first injection is designated day 0. Starting from day 0 of injection rats were kept on basal diet and water *ad libitum* for 9 weeks, then blood samples were collected from orbital vein sinus for complete blood picture (CBC) analysis.

2.4.1.3. *Experimental design*

Rats were randomly divided into 2 main groups, group1: (negative control) 10 rats received a balanced diet with biweekly (i.v.) saline injection for 3 weeks, group2: 30 rats injected with NMU as described previously for induction of AML. After the 9th week of the day, 0 rats of group2 were randomly subdivided into 3 subgroups. Group 2a: (AML group) 10 rats served as the positive control group, group2b: 10 rats received daily oral dose 50 μ g/kg body weight MNPs (Shirband et al., 2014) for 6 weeks (AML+MNPs group) and finally, group 2c: 10 rats received a daily oral dose of 50 μ g/kg body weight FMCS (AML+ FMCS group) for 6 weeks.

2.4.1.4. *Sampling*

At the end of the 6th week of NPs treatment, animals were sacrificed under isoflurane anesthesia. blood samples were collected from the hepatic portal vein in two separated tubes; the first tube contained EDTA to

collect whole blood while the second type was used for separating serum by allowing blood samples to stand for 15 min at 37°C, then centrifugated at 3000 rpm for 15min where the clear serum was separated and immediately stored at -20 in a clear plastic Eppendorf till analysis. Liver and spleen tissues were excised, washed, and weighted; bone marrow tissues also were excised from the bone. Liver, spleen, and bone marrow specimens were kept in 10% formalin solution for microscopic examination.

2.4.2. *Biological assessment*

Bodyweight was recorded weekly, and the change in body weight was calculated at the end of the experiment. Liver and spleen weight were measured immediately after sacrificing.

2.4.3. *Biochemical analysis*

Serum transaminases (ALT, AST) and lactate dehydrogenase (LDH) activities were determined by colorimetric method according to Reitman and Frankel (1957) and Moss et al. (1987) respectively. Uric acid was determined in serum by an enzymatic colorimetric method according to Barham and Trinder (1972). Beta 2 Microglobulin was analyzed by the automated Cobas6000 system. Also, CBC was performed using Sysmex (Automated Hematology Analyzer XT 2000i/XT-1800i).

2.4.4. *Immunophenotyping for CD34 and CD38 detection*

The whole blood lysis staining method was performed using Multicolor flow cytometry (Coulter Epics, Navios, USA). Navios software in Flow Cytometry Laboratory, Bone Marrow Transplantation Laboratory Unit (BMT Lab Unit), Clinical Pathology Department, NCI, Cairo University.

Monoclonal antibodies (mAb) were used to identify cells by detecting specific antigens expressed by these cells. For the detection of CD34 expression phycoerythrin (PE)-conjugated antibodies were used; (CD34PE, 2ml/100 test, Cat.no.: A32535, Beckman Coulter, Miami) and For CD38 detection, fluorescein isothiocyanate (FITC)-conjugated antibodies were used; (CD38 FITC, 1ml/50 test, Cat.no. 562125). The flow cytometer detects fluorescently emitted light of different wavelengths from each cell using mAb that is conjugated to different fluorochromes (FITC for green light emission and PE for red/orange light emission), one can detect the emission of light from single cells that bind these mAb (Jennings and Foon, 1997).

2.4.5. *Detection of Bcl-2 methylated status*

2.4.5.1. *DNA extraction and preparation*

Genomic DNA was extracted from 10 mm whole blood sample using a QIAamp DNA FFPE tissue kit (Qiagen, Valencia, CA, USA). A universally methylated reference sample was prepared using (M.SssI, New England Biolabs, Ipswich, MA, USA). Genomic DNA of rat was treated with M.SssI (0.05 units/mL final concentration) and S-adenosyl methionine (SAM) overnight, followed by another overnight incubation with an additional M.SssI (0.09 units/mL final concentration) and SAM. The M.SssI-treated DNA was

Table 1. The primer sequences for Bcl-2; caspase-3; and β - actin.

Primers
Bcl-2 F 5'-CCTGTG GAT GAC TGA GTA CC-3'
Bcl-2 R 5'-GAGACA GCC AGG AGA AAT CA-3'
Caspase-3 F 3'- TGTGAGCGGTTGTGGAAGAGT-5'
Caspase-3 R 3'- AATGGGGAAGAGGCAGGTGCA -5'
β -actin F 5'-GTGACATCCACCCAGAGG-3'
β -actin R 5'-ACAGGATGTCAAACTGCC-3'

purified using a DNA Clean and Concentrator kit (Zymo Research, Irvine, CA, USA).

2.4.5.2. Sodium bisulfite modification and DNA recovery

Two micrograms of genomic and M.SssI treated DNA were sodium bisulfite modified using a Zymo EZ DNA Methylation Kit (Zymo Research, Irvine, CA, USA) as kit described. Sodium bisulfite converts unmethylated cytosines to uracils but does not affect the methylated cytosines.

2.4.5.3. Quantitative polymerase chain reaction detection of Bcl-2 promoter methylation status

After sodium bisulfite conversion, genomic and M.SssI treated DNA were amplified by fluorescence-based quantitative polymerase chain reaction (qPCR) using an ABI7900 unit. Serial dilutions of M.SssI treated DNA were included on each plate to generate a standard curve. PCR amplification was performed with a final reaction mixture of 25 mL consisting of 600 nmol/L of each primer, 200 nmol/L probe, 200 mmol/L dNTPs, 3.5 mmol/L MgCl₂, 10X TaqMan buffer without Uracil DNA glycosylase (AMPerase), 10X stabilizer, and water.

Bisulfite converted DNA was amplified at 95°C for 10 min, followed by 50 cycles at 95°C for 15sec and 60°C for one minute. Primers and probes, designed specifically for bisulfite converted DNA, were used for Bcl-2 and Col2a1, a reference gene to normalize for input DNA. The Bcl-2 and Col2a1 primer and probe sequences are listed in Table 2. Bcl-2 primer and probe were designed to contain seven CpG dinucleotides in a CpG island located in the first exon of Bcl-2. Primers and the probe were designed using Primer Express Software ABI 7900 in a region of the Col2a1 gene that lacks any CpG dinucleotides to allow for equal amplification, regardless of methylation levels. The percentage of fully methylated molecules at a specific locus was calculated by dividing the Bcl-2: Col2a1 ratio of a sample by the Bcl-2: Col2a1 ratio of M.SssI-treated DNA and multiplying by 100.

2.4.6. Statistical analysis

Data were statistically analyzed by Statistical Package for Social Science (SPSS) version 16.0. Values were presented as mean ± standard error (S.E.). Statistical differences between groups were performed using one-way Analysis

of Variance (ANOVA), the mean difference was significant at the ($p < 0.05$) level according to Levesque (2007).

2.4.7. Histopathological analysis

Organs of each rat were immediately washed in saline and embedded in 10% neutral buffer formalin, then fixed in Paraffin sections of suitable thickness and stained with hematoxylin and eosin (H&E) for histopathologic examination.

3. Results and Discussion

3.1. Characterization of nanoparticles

The characterization technique used for MNPs and MFCS aimed to not only determine the physicochemical properties that influence its anticancer activity but also how core-shell nanostructure formation affects cancer cells. Characterization was classified according to its physicochemical properties into three classes namely morphology identification and index classes.

Morphology classes were carried out by 3D SEM image and 2D TEM image for MNPs and MFCS as shown in Figures 1 and 2 respectively. SEM and TEM images illustrated the mono dispersion of MNPs with spherical shape and size range from 15 to 35 nm. While MFCS has a spherical shape with a very sharp edge of the shell and a spherical shape of the core. However, the TEM image confirms the formation of a core-shell nanostructure with a spherical core size of 50 nm and shell size of 20 nm.

Identification class was used to confirm the formation of MNPs and MFCS without any contamination resulting from the synthesis method and confirm that magnetite has the same chemical and crystal form after conversion to nano size. The result from the XRD pattern of both MNPs and MFCS as shown in Figure 3 illustrated the high purity of them where there are 5 very sharp strong peaks characterized to MNPs according to ICDD database (COD 2101926) with cubic lattice, volume [CD] 577.41 and S.G. fd-3m (227). Folic acid is characterized by one very sharp peak at 2theta 22.154° according to ICDD database (COD 5900002) with tetragonal lattice, volume [CD] 151.94, and S.G. p-421m (113). Presences of identity peaks of both magnetite and folic acid confirmed the formation of core-shell structure. EDX was used as elemental analysis

Table 2. Primer and probe sequence of promoter methylation.

Primers	Probe sequence 5' to 3'
Bcl-2	6FAMCTAAAAATAACTTCTCTCGTCGCT-MGB*
F3'GGATATTTTTGTAAGTCGCGACG5'	
R5'ACCTATAATCCACCTAACCTCCG3'	
Col2a1	6FAM-ACCTCTAATCCCTCCAAA-MGB*
F3'GGTATTTTTGTGTTTGAAGAGTAGTTG5'	
R5'CCTTCTCTCTCTTAACTCAA3'	

*MGB refers to a Minor Groove Binder non-fluorescent quencher in the 3' terminus of the probe.

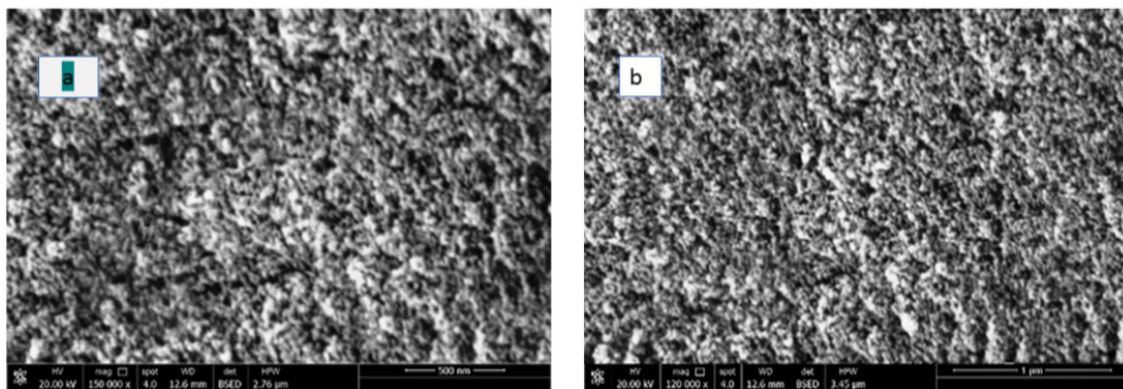


Figure 1. SEM image for a) MNPs and b) MFCS.

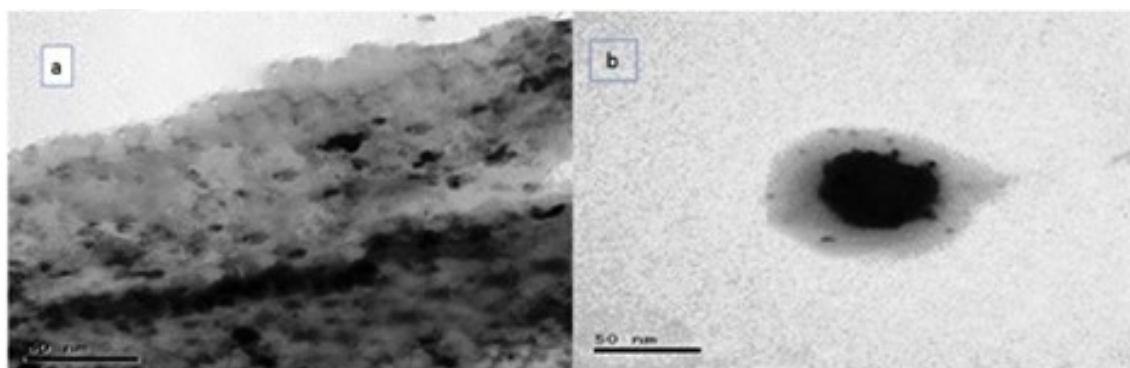


Figure 2. TEM image of a) showing MNPs b) showing MFCS.

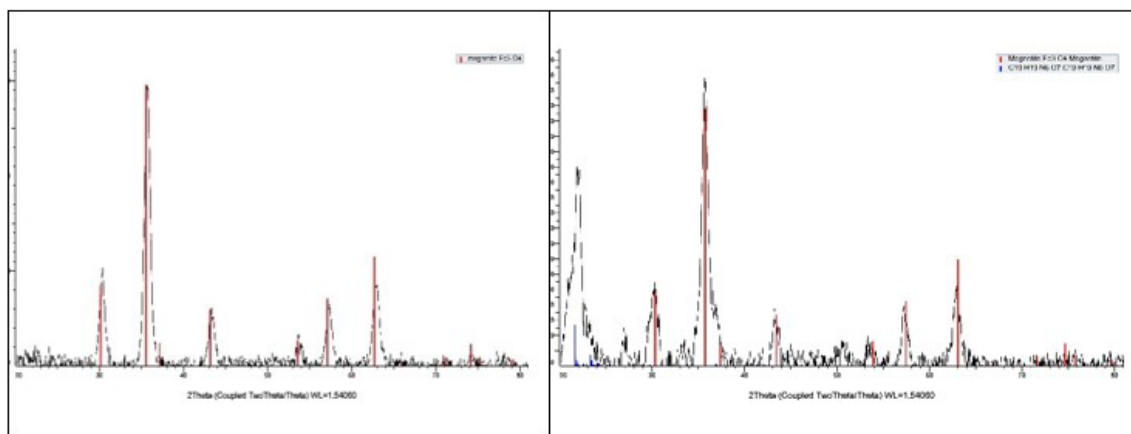


Figure 3. The XRD pattern of left MNPs and right MFCS magnetite nanoparticles with red lines and folic acid with blue lines.

tools to evaluate the purity and sensitivity of the synthesis method of nanomaterials. However, EDX results as shown in Figure 4 illustrated the high purity of both MNPs and MFCS. AFM measurement showed in Figure 5 was done just for MFCS to confirm the shape, size, concentration, and agglomeration obtained from TEM and SEM images. AFM images illustrated the spherical shape of magnetite nanoparticles core (red color) with the shell of folic acid

(yellow color). MFCS almost separated from each other and do not tend to agglomeration or concentrated in a certain area.

BET Surface area and average pore size of MFCS have been measure after degassing by vacuum heating at 80°C for 1 hour. BET surface area was measured for MNPs, folic acid, and MFCS to evaluate the chemical activity of them where the increased BET surface area value leads to an

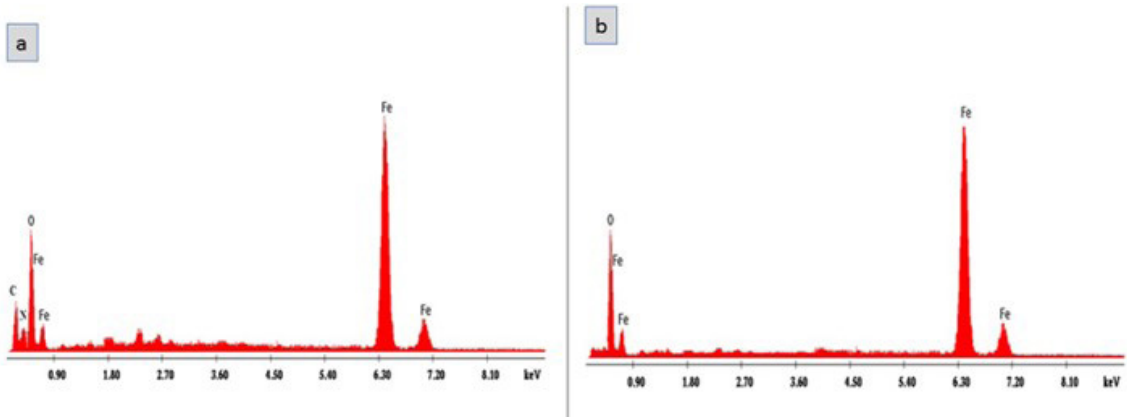


Figure 4. EDX of a) MNPs and b) MFCS confirm the formation of NPs without any contamination.

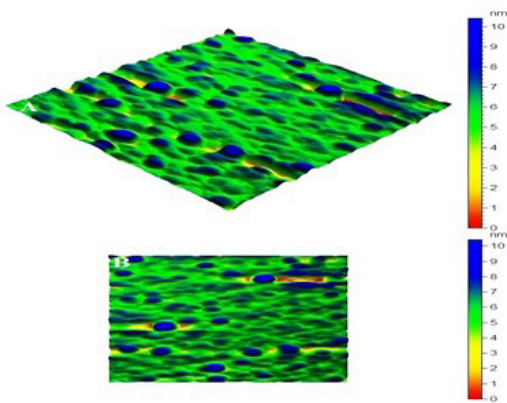


Figure 5. AFM images of MFCS, where A) 3D AFM image and B) top view one.

increase in chemical activity. BET surface area as shown in Figure 6 was 67.1, 39.56, and 141.293 m²/g for MNPs, folic acid, and MFCS, respectively. The increase in BET surface area of MFCS more than magnetite nanoparticles and folic acid leads to enhance the anti-cancer effect, which may be related to increasing the contact with the cancer cell wall. However, MNPs, folic acid, and MFCS have IV-type isotherm with mesoporous capillary type. The average pore size by DA method was 1.75, 2.44, and 1.70 nm for MNPs, folic acid, and MFCS, respectively. The decreased average pore size of MFCS was due to precipitation of the folic acid (shell) on magnetite nanoparticles (core) and blocking its pores.

3.2. *In vitro* study

3.2.1. IC₅₀

The present result indicated that MNPs and MFCS had less effect on SNU-182 cells compared to thalidomide drug, meanwhile, both nanoparticles had a remarkable effect on K562 cell line. On the other hand, IC₅₀ for MFCS was significantly lower than that of MNPs for SNU-182 and

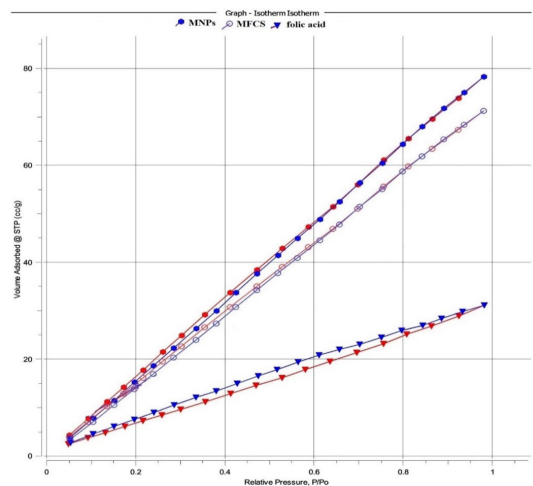


Figure 6. Isotherm curve of MNPs, folic acid, and MFCS.

K562 cells and significantly increased for THLE2 compared to MNPs and thalidomide drug suggesting that MFCS have a powerful cytotoxic effect on hepatic carcinoma and leukemia cell line with less cytotoxic effect on the normal hepatic cell line Figure 7.

Our results in the same line with the study of (Namvar et al., 2014) who showed that exposure of Jurkat cells (leukemia cell line) and HepG2 cells (liver cancer) to MNPs resulted in significant cytotoxicity, with an apoptotic response, but not in normal liver cell line, providing new opportunities for safe delivery of MNPs and application in anticancer therapy. Novotna et al. (2012) examined the effect of superparamagnetic iron oxide nanoparticles on human bone marrow mesenchymal stromal cells (hBMSCs) from two donors. Their results showed that hBMSCs-2 were sensitive to these nanoparticles; moreover, increased oxidative injury to lipids, proteins, and DNA was detected in cells from both donors.

In addition, the study of Peng et al. (2016) demonstrated that MNPs were the effective drug delivery vehicles to deliver wogonin drug to leukemia cells. Through increasing

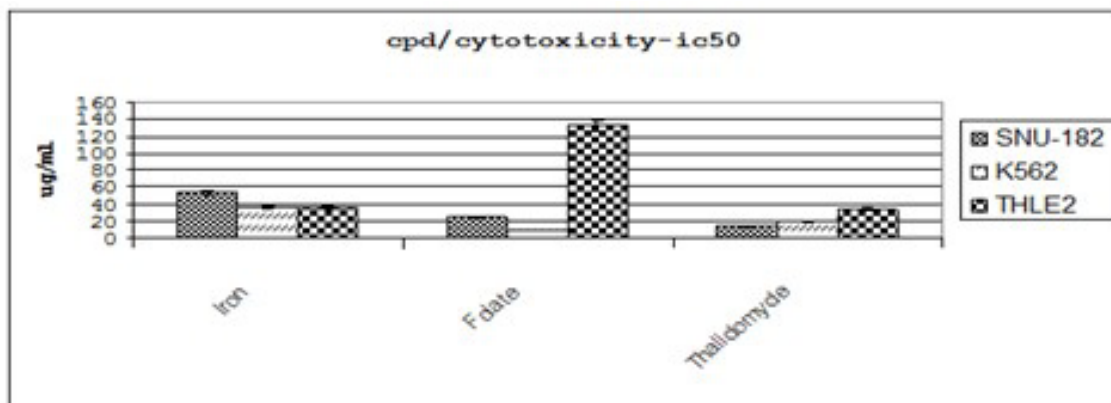


Figure 7. The half-maximal inhibitory concentration (IC50) for MNPs, MFCS against thalidomide reagent expressed as ug/ml.

cells arrested at G0/G1-phase and inducing apoptosis, MNPs could enhance the therapeutic effects of wogonin on leukemia cells. These findings indicated that loaded MNPs could provide a promising way for better leukemia treatment.

Folate capping nanoparticles induced a much powerful effect than MNPs. This result was confirmed by the previous work of Fang et al., (2017) who showed that FA with selenium nanoparticles significantly enhances selective cellular uptake by liver cancer (HepG2) cells which were higher than those for the SeNPs. Also, folate-conjugated nanoparticles have great potential for cancer detection and treatment. Capped folate nanoparticles could diagnose and treat non-invasive cancer, as well as targeting tumors directly through their overexpressed folate-receptors. Folate-receptors are highly overexpressed on the surface of many tumor cell types (Hashemian and Mansoori, 2013).

Moreover, FA treatment upregulated the expression of E-cadherin in nasopharyngeal cancer (NPC) cells via activating FR- α . E-cadherin is a well-known mediator that has a pivotal role in cell-cell adhesion and epithelial development. E-cadherin expression is found to be greatly decreased in many tumors including NPC cells (Liu et al., 2017).

The current results revealed that folic acid-modified nanoparticles caused worse damage to cancer cells than to normal cells. folic acid coupled to the surface of iron oxide immobilized the surfaces of magnetic nanoparticles. This complex improves cell internalization and targeting of cancer cells. Furthermore, our results showed that the uptake of folic-acid modified nanoparticles by cancer cells especially leukemia cells was also much higher than normal cells and was more effective than the Thalidomide drug. This modification can be a good strategy used for the successful targeting of cancer cells.

3.2.2. mRNA expression levels of Bcl-2 and caspase-3

The present results showed in Figure 8 strongly supported the apoptosis induction in MNPs and MFCS treated K562 and SNU-182 cells as compared with the untreated cells indicated by up-regulation of caspase-3 together with a down-regulation of anti-

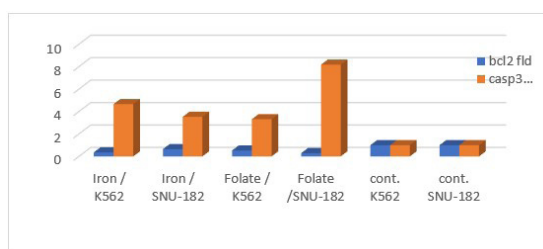


Figure 8. Protein expressions of bcl-2 and casp-3 incubated with MNPs and MFCS analyzed using RT-PCR. The control (beta-actin) images are re-used for illustrative purposes.

apoptotic gene Bcl-2. This pattern strongly supported the cytotoxic effect of MNPs and MFCS.

The present results showed that the induction of apoptosis by the cytotoxic dose of MNPs and MFCS mediated G2/M phase arrest and undergoing apoptosis via cascade reaction. From this point, the results of this study demonstrated that the effects of MNPs and MFCS on apoptosis induction, cell cycle progression in K562 and SNU-182 cell lines were significantly increased in a dose-dependent manner, by up-regulation of Caspase-3 mRNA expression and down-regulation of Bcl-2 mRNA expression. On the other hand, apoptosis was still stimulated through the extrinsic apoptotic pathway so that we could see the up-regulated levels of Caspase-3 mRNA expression that previously confirmed by Chiang et al., (2014).

Namvar et al., (2014) also showed that MNPs increased the activity of caspase-9 and caspase-3 in a time-dependent manner. According to Wang et al. (2017), MNPs treatment contributed to apoptosis in (NSCLC) lung cancer cells, as evidenced by activation of the caspase 3-signaling pathway, which was accompanied by downregulation of the anti-apoptotic proteins Bcl-2. The combination therapy of MNPs with actein showed a stronger inhibitory role in cancer cell proliferation, triggering considerable apoptosis of lung cancer cells.

Caspase-3 activity was confirmed by the study of Akbarzadeh et al. (2018) who reported that the folate-

modified NPs have a high level of cytotoxicity on KB nasopharyngeal carcinoma cells when compared to the NP itself. The reason behind this may be because of the targeting effect of FA that is based on the specific identification of folate receptors on the surface of KB cells.

3.3. *In vivo* study

The results of *in vitro* study confirmed the cytotoxic and apoptotic effect of MNPs and MFCS on hepatic carcinoma and leukemia cell lines. The most significant effects were observed on leukemic cells. Therefore, AML induction was used as an animal model to investigate the effect of MNPs and MFCS as anticancer agents.

3.3.1. Biological assessments

Although rats of all groups increased in their body weight by the end of the experiment, the average body weight gain in AML groups was significantly ($P \leq 0.05$) decreased than the control group, there were non-significant ($P > 0.05$) differences between the group that administered NMU alone and NMU groups treated either by MNPs or MFCS. Gross evaluation of the liver and spleen from the AML rats indicated that these organs were abnormally enlarged in appearance and their weight was significantly higher than normal control rats. Rats of AML + MNPs or AML + MFCS showed a significant ($P \leq 0.05$) decrease in liver and spleen weights comparing to rats that were exposed to NMU alone, this reduction is more significant for MFCS treated group and nonsignificantly different from that of the control group Table 3.

Torelli et al. (1997) reported that a series of clinical symptoms, such as anorexia, weight loss, muscular atrophy, tissue wasting, and altered organ function which is known as cachexia is frequently observed in cancer and makes a decisive contribution to morbidity and mortality.

Chang et al. (2012) hypothesized that the decrease in body weight gain in AML rats induced by NMU administration is due to that rats were suffering from a lack of appetite. The liver and spleen were enlarged due to an invasion of leukemic cells and their build-up in these organs.

In acute myeloid leukemia, extramedullary infiltration by leukemic cells may cause splenomegaly or hepatomegaly. In the study made by Chang et al. (2016) hepatomegaly and splenomegaly were observed in 48% and 45% of patients respectively. The majority had mild to moderate hepatosplenomegaly.

Previously, Kumari et al. (2013) observed non-significant decreases in feed intake in MNPs treated animals with no significant differences in body weight. Also, Elsayed et al. (2014) showed that treatment of anemic rats with MNPs and folate coated MNPs caused loss of appetite and severe lethargy with no significant change in body weights and different relative weight of liver and spleen.

3.3.2. Complete blood count (CBC) in experimental groups:

Table 4 indicated that the total count of WBCs was significantly ($p \leq 0.05$) higher in the NMU-treated group, in contrast, other hematological data (RBCs, Hb, and platelet counts) were lower than the control group. Concerning the differential count (percentages of each type of WBCs), the

Table 3. Body weight gain, liver and spleen weights.

Groups	Body weight gain (g)	Liver weight (g)	Spleen weight (g)
Control	104.62 ± 1.22 ^a	6.26 ± 0.44 ^a	0.77 ± 0.01 ^a
AML	50.12 ± 9.62 ^b	8.87 ± 0.22 ^b	1.14 ± 0.05 ^b
AML + MNPs	54.25 ± 5.53 ^b	7.33 ± 0.33 ^c	0.88 ± 0.02 ^c
AML +MFCS	61.62 ± 4.37 ^b	6.68 ± 0.36 ^{ac}	0.79 ± 0.03 ^{ac}

Values are expressed as means ± S.E., n= 8, There was no significant difference between means have the same letter in the same column ($P \leq 0.05$)

Table 4. Complete blood count (CBC).

Groups	Control	AML	AML + MNPs	AML +FMCS
HB (g/dl)	13.75 ± 0.37 ^a	10.62 ± 0.19 ^b	12.72 ± 0.17 ^a	13.05 ± 0.56 ^a
RBCs × 10	7.89 ± 0.20 ^a	6.54 ± 0.11 ^b	6.90 ± 0.12 ^{bc}	7.31 ± 0.24 ^c
Platelets	525.50 ± 14.28 ^a	249.25 ± 5.49 ^b	361.12 ± 19.45 ^c	431.87 ± 23.67 ^d
WBCs	4.76 ± 0.54 ^a	9.99 ± 0.45 ^b	6.65 ± 0.93 ^c	5.87 ± 0.51 ^{ac}
Neutrophils	41.73 ± 2.36 ^a	7.65 ± 0.82 ^b	21.64 ± 1.87 ^c	28.91 ± 1.19 ^d
Lymphocytes	42.41 ± 0.97 ^a	17.48 ± 2.47 ^b	23.23 ± 2.45 ^c	30.96 ± 1.18 ^d
Monocytes	4.44 ± 0.39 ^a	0.82 ± 0.04 ^b	1.38 ± 0.24 ^b	2.22 ± 0.29 ^c
Eosinocytes	6.28 ± 1.04 ^a	1.06 ± 0.19 ^b	3.90 ± 0.56 ^c	4.57 ± 0.84 ^{ac}

Values are expressed as means ± S.E., There was no significant difference between means have the same letter in the same row ($P \leq 0.05$)

results indicated that administration of NMU significantly decreased the percentage of neutrophils, lymphocytes, monocytes, and eosinocytes more than the control group. The treatment of AML rats with MNPs or MFCS significantly decreased the elevated WBCs count and increased the RBCs, Hb, and platelet counts, moreover, ameliorated the differential count of WBCs comparing to rats treated with NMU alone.

The elevated WBCs count indicated the development of leukemia and the decreased values of RBCs and Hb indicating a tendency to anemia. Our results suggest that the administration of NMU to rats induces an increase in the WBCs count without affecting the neutrophil index. The increased production of leukemia blasts led to a reduction in the percentage of normal neutrophils and implied a direct correlation between leukemia blasts and the number of WBCs (Ghosh et al., 2003).

AML is a malignant disorder of the blood characterized by blocked or impaired differentiation of hemopoietic stem cells. This resulted in an abnormal accumulation of immature precursors and a suppression of growth and maturation of cells involved in normal hemopoiesis (Smith et al., 2004).

Our hematological results were comparable with that of Chang et al. (2016), who reported that anemia is a constant feature in all acute leukemias, and the majority of cases are due to bone marrow infiltration, leading to decreased production and rarely due to decreased red cell life span and autoimmune destruction. Among adult patients with AML, 5% to 30% present with hyperleukocytosis (increase the WBCs count) and symptoms of leukostasis which increased the blood viscosity and caused aggregation of leukemic cells in the microcirculation. Moreover, 95% of AML patients developed thrombocytopenia and a low platelet count.

MNPs are available for the treatment of iron deficiency in the clinic. It is recently reported that MNPs show an anti-leukemia effect due to increased iron-catalyzed ROS and low expression of the iron exporter ferroportin 1 (FPN1) resulted in enhanced susceptibility of AML cells to iron oxide nanoparticles. The iron-based nanoparticles were modified for enhancing their anticancer efficacy. It is reported in the current work that the anti-leukemia effect of iron oxide is enhanced by being coated on folate nanoparticles (core shell). Furthermore, the magnetic field itself can play anti-leukemia effects by increasing ROS production. Therefore, the application of iron-based nanoparticles directed by magnetic field may provide

an approach to the prevention and treatment of central nervous system infiltration of leukemia. The magnetic fields not only concentrate nanoparticles but also promote the production of ROS in cells to play anti-leukemia effects (Wang et al., 2019).

Treatment of AML rats with either MNPs or MFCS improve all CBC parameters, moreover, CBC of MFCS treated rats nearly approach that of normal control. El Sayed et al. (2014) observed that Some doses from MNPs or folate coated MNPs improve the blood picture of anemic rats within 2 weeks. Vieira et al. (2006) study the MNPs that could potentially be used as novel therapeutic agents in the treatment of protein myeloid aggregation-associated human pathologies

3.3.3. AST, ALT, and LDH activities and uric acid level in experimental groups

The effect of NMU-induced leukemia and treatment with nanoparticles on rat's liver function in terms of serum AST and ALT as well as serum LDH and uric acid is presented in Table 5. Induction of AML caused a significant increase in the levels of serum AST and ALT enzyme activities, these activities were significantly decreased when rats are treated with MNPs or MFCS NPs. Concerning serum LDH and uric acid, the data indicated that their levels in AML rats were higher than the normal values of the control group, whereas rats that were exposed to MNPs or FMCS NPs showed significantly decreased level than AML rats.

Mathews et al. (2008) showed elevated liver function tests in AML patients which normalized with chemotherapy administration suggesting that AML was the causative effect of the hepatitis-like picture. Also, the study of Matsueda et al. (1998) identified a patient with AML as having leukemic liver disease.

Under rapid proliferation and immaturity of tumor cells, LDH is released due to multiple cytokine activity and damage of the cell membrane. Any change in lactate dehydrogenase level in blood is a reflection of the presence of cell damage. This change may be due to an altered amount of the enzyme forming tissue, as a defect in the rate of enzyme synthesis, or due to a defect in the permeability of the cell member as a result of physiological stress. In acute leukemia, the level of LDH is elevated due to cell destruction and tumor turnover. (Fikry, 2017).

Hafiz and Mannan (2007) found that elevated LDH activity was highly correlated with higher white blood cell count and uric acid, lower platelet count, and larger spleen size. Furthermore, Al-Saadoon et al. (2003) reported that

Table 5. AST, ALT, Uric acid, and LDH levels.

Groups	AST	ALT	LDH	Uric acid
	(U/l)	(U/l)	(U/l)	(mg/dl)
Control	207.20 ± 1.60 ^a	49.55 ± 0.95 ^a	1012.7 ± 1.52 ^a	1.32 ± 0.02 ^a
AML	484.56 ± 3.21 ^b	166.73 ± 4.02 ^b	2652.5 ± 21.8 ^b	2.14 ± 0.08 ^b
AML + MIO	362.47 ± 1.59 ^c	92.26 ± 2.10 ^c	1690.1 ± 30.3 ^c	1.79 ± 0.11 ^c
AML +FO-MIO	239.81 ± 1.67 ^d	60.90 ± 1.33 ^d	1129.2 ± 5.3 ^d	1.48 ± 0.08 ^a

Values are expressed as means ± S.E., There was no significant difference between means have the same letter in the same column (P<0.05).

high LDH level in acute lymphoblastic leukemia (ALL) was correlated with leukocyte counts and blast cells. Jing et al. (2011) illustrated that there was a negative correlation between LDH activity and red blood cells and platelet count.

Elevation of LDH in malignancy tumor may be explained by acidification of the extracellular water space by lactate and the subsequent activation of tumor invasion or, low pH microenvironment may increase cancer cell resistance to hypoxia-induced apoptosis by protecting mitochondria from oxidative stress. Finally, overexpression of LDH, especially LDH-5, reflects an upregulated hypoxia-induced factor pathway, which regulates glycolysis, angiogenesis, resistance to apoptosis, and even cancer metastasis (Fikry, 2017).

Kumari et al. (2013) showed that activation of the hepatotoxicity marker enzymes, AST and ALT, was recorded in serum and liver of AML group. Similarly, enhancement of LDH activity was observed in serum and liver; however, a decrease in enzyme levels was observed in kidneys of MNPs-treated rats. Exposure to nano-size particles at acute doses may cause adverse changes in animal biochemical profiles. Jarahian et al. (2018) reported that MNPs even in the presence of a constant magnetic field has affected reversible toxic effects on liver activity, and over time these effects had been corrected.

Determination of serum uric acid level is useful for detecting hyperuricemia and in diagnosing leukemia, gout, polycythemia, and renal dysfunction (Hafiz and Islam, 2009). Yamauchi et al. (2013) reported that uric acid in serum is produced by the breakdown of the cellular nucleic acids of leukemia cells and may be a marker of disease aggressiveness. In the present study, high serum uric acid level was found in AML group which was consistent with the findings reported by Tsimberidou et al. (2008).

On the other hand, the current results observed that folate core shell nanoparticles cause reduction of MNPs toxicity that also confirmed by previous work of Ruiz et al. (2015) who show that both, dimercaptosuccinic acid (DMSA) and PEG-coated MNPs undertake a quick transformation process under moderate doses in rats are good candidates for biomedical applications such as cancer research and clinical diagnosis since the possible toxicity associated to MNPs accumulation is reduced.

The toxicity and biodistribution of super magnetite iron oxide coated with polyethylenimine did not affect the hepatic and renal functions in rats and the toxicity was very low. Tissue distribution is principally influenced by the size of iron oxide nanoparticles. It has been known that smaller particles tend to stay in blood circulation longer, and, however, larger nanoparticles (over 50 nm in

diameter) are more readily sequestered by Kupffer cells in the liver and macrophages of the spleen (Yu et al., 2018).

3.3.4. Beta -2-microglobulin (B2M) and Relative Bcl-2 methylation in experimental groups

Results presented in Table 6 showed that AML induced by NMU injection caused a significant increase in β -2microglubulin level with a significant reduction in relative Bcl-2 methylation percent. Treatment of AML with either of NPs caused a significant reduction of β -2microglubulin and significant elevation in Bcl-2 methylation percent compared to AML group. Furthermore, the reduction of β -2 microglobulin caused by MFCS NPs nearly reached the level of normal control. Meanwhile, MFCS caused elevation of Bcl-2 methylation that exceeds normal control.

Beta-2-microglobulin (B2M) is a subunit of the major histocompatibility complex (MHC) class I molecule; it is found on the surface of all nucleated cells and is especially abundant in lymphocytes and monocytes. Under normal physiological conditions, some amount of B2M may be secreted into circulation from or as a result of the intracellular release and is removed from blood predominantly by the kidneys. Thus, the net concentration of serum B2M is determined by its generation and secretion into serum, as well as its elimination by the kidneys, so that serum B2M concentration increases with an elevated turnover of cells and/or reduced kidney function. Therefore, in people without kidney disease, elevated B2M serves as a marker of altered cell proliferation (Prizment et al., 2017).

B2M is a marker of severity and progression in AML. Thus, serum B2M levels have prognostic value in AML patients. Elevated levels of B2M indicated high turnover of leukemic cells and low levels after therapy may indicate the completeness of remission in terms of the leukemic cell turnover better than the absolute cell counts in the blood (Dokwal et al., 2016). In the present study, treatment with MNPs and MFCS ameliorated B2M level, indicating decreased cell turnover and improved AML condition.

In cancer cells, Bcl-2 is hypomethylated leading to a high Bcl-2 expression. These observations are relevant because high levels of Bcl-2 are observed in the metastatic state of various types of cancer including colon cancer. Hypermethylation of promoters is a recognized mechanism by which the expression of tumor suppressor genes is inhibited during cancer development. In contrast to hypermethylation of tumor suppressor genes, a region in the first exon of Bcl-2 oncogene is completely demethylated allowing high levels of Bcl-2 expression in B-cell chronic

Table 6. Beta -2-microglobulin and Relative Bcl-2 methylation.

Groups	Beta -2-microglobulin (ng/mL)	Relative Bcl-2 methylation (%)
Control	1.14±0.08 ^a	96.07±1.13 ^a
AML	2.24±0.11 ^b	68.65±3.96 ^b
AML + MNPs	1.58±0.10 ^c	99.60±0.36 ^a
AML +MFCS	1.31±0.07 ^a	149.7±0.31 ^c

Values are expressed as means ± S.E., There was no significant difference between means have the same letter in the same column ($P \leq 0.05$).

lymphocytic leukemia (Cho et al., 2012). Aberrant promoter methylation has been proposed as a prognostic marker of cancers, and the extent of methylation in a tumor is associated with disease progression, recurrence, and survival rates in various types of cancer (Liu et al., 2008).

The present work indicated that NMU-induced leukemia exhibited a higher methylation percent of the Bcl-2 promoter in rats consuming MFCS, compared with MNPs. Interestingly, there are no previous studies that investigated the effect of NPs on methylation of Bcl-2, promoter in animal models of cancer. Meanwhile, many studies concerned with the effects of folic acid supplementation as a methyl donor and focused on either preventing or promoting cancer. Following Cong et al. (2012) folic acid supplementation can prevent Bcl-2 hypomethylation induced by hyperhomocystein treatment, resulting in a decreased Bcl-2 expression.

3.3.5. Immunophenotyping for CD34 and CD38

Flow cytometry analysis of the blood cell surface markers showed in Figure 9 demonstrated that the percentage frequency of each fraction expressing of cells CD34 and CD38 antigens were 99.8% of gated cells (negative) and no significant for both CD38 FITC and CD34 PE. Whereas the CD34 PE was positive on 0.4% and the CD38 FITC was positive on 0.1% of gated cells, for AML group, that was highly significant compared to control group. While the histogram showed MNPs- treated group had no significant difference for both the CD34 PE (0.4%) of gated cells and the CD38 FITC (0.1%) of gated cells compared to AML group. Whereas MFCS treated group had a highly significant difference in both CD34 PE drop for 0.4% to 0.2% and CD38 FITC disappear 0.1% to zero% compared to AML group.

CD34 is a cluster-of-differentiation molecule first described by Civin et al. (1984) in a cell surface glycoprotein and is encoded by the CD34 gene. CD34 is expressed by leukemia blasts only for a subset of patients with AML. CD38 is a type II glycoprotein that was originally described as a lymphoid cell surface differentiation marker (Orციანი et al., 2008). CD34 and CD38 expression can serve as a specific biomarker for the prognosis of this subset of leukemia (Jiang et al., 2016).

CD38 expression is an important prognostic factor in B-cell chronic lymphocytic leukemia. It is an important prognostic factor associated with a high incidence of lymph node involvement, lower hemoglobin level, hepatomegaly, and high β 2M level. In myeloid cells, CD38 is expressed on immature precursors and can be upregulated using all-trans retinoic acid. Its presence has been associated with a better prognosis in acute myeloid leukemia (AML), CD38 has been reported to play a complex role in lymphocyte proliferation. Ligation of CD38 using an agonistic monoclonal antibody produced diverse responses manifested as growth or apoptosis. CD38 ligation on mature B cells protects against apoptosis and up-regulated the expression of the Bcl-2 proto-oncogene. In contrast, ligation of the CD38 molecule suppressed the growth of immature B cells in the bone marrow micro-environment. The higher the percentage of CD38 cells, the more aggressive the disease—imply that CD38 expression is a parameter for disease progression. (Ibrahim et al., 2001). Moreover, Omstead et al. (2020) results highlight a promising cancer treatment option in CD38-targeted nanoparticles and emphasize that targeting succeeds in vitro. As controlling the expression of CD34 and CD38 by MFCS and MNPs, the progression of AML could be inhibited by mitigating the other biochemical consequences.

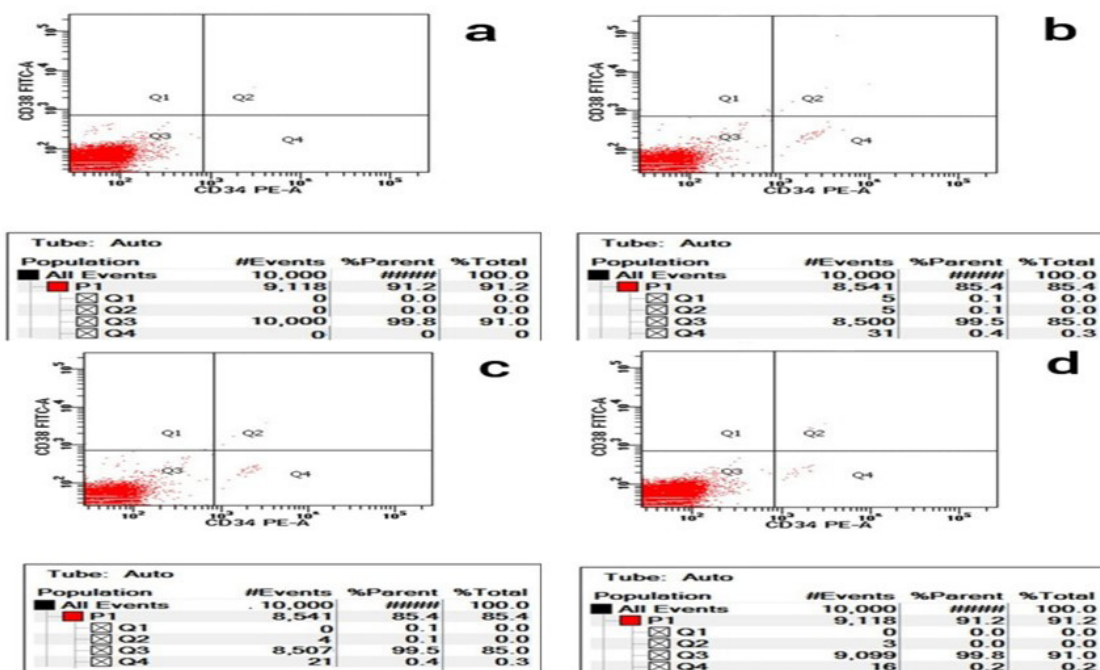


Figure 9. Histogram for immunophenotyping for CD34 and CD38.

3.3.6. Histopathological analysis

The result of microscopic examination illustrated in Figures 10, 11, 12, and 13 confirmed the results obtained

from the biochemical analysis. As shown in Figure 11, AML induced by NMU caused severe portal lymphocytic infiltrate, moderate ballooning degeneration, and piecemeal

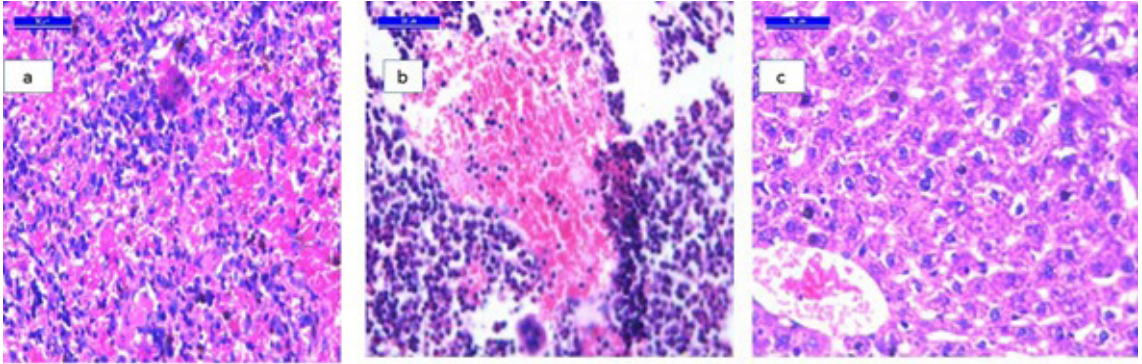


Figure 10. a) Section from liver tissue of normal control group showing normal liver tissues preserved architecture, no portal tract fibrosis, no piecemeal necrosis (H&E, X 400). b) Section from bone marrow tissue of normal control showing normal bone marrow at medium magnification. Note the presence of megakaryocytes, erythroid islands, and granulocytic precursors (H&E, X 400). c) Section from spleen tissue of normal control group showing spleen, granulocytes, erythropoietic cells, lymphocytes, and hemosiderin-laden macrophages are present amid the splenic cords (H&E, X 400).

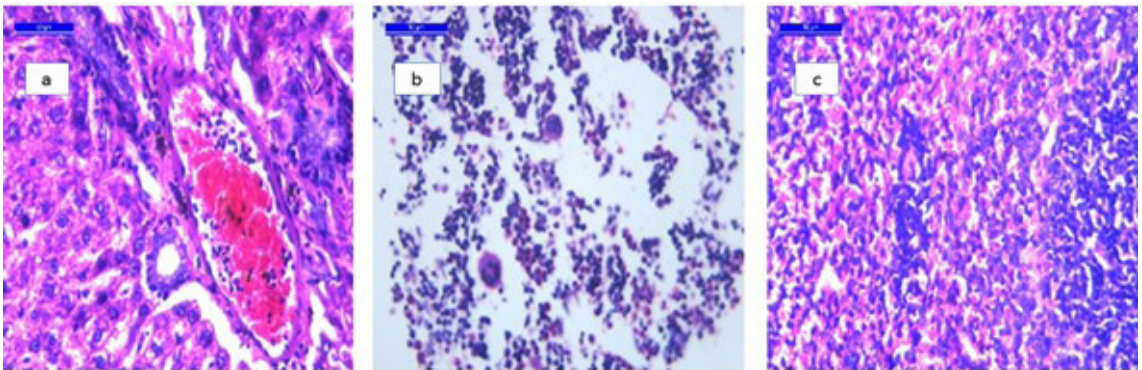


Figure 11. a) Section from liver tissue of AML group showing Severe portal lymphocytic infiltrate, moderate ballooning degeneration, and piecemeal necrosis (H&E, X 400). b) Section from bone marrow tissue of AML showing aplastic anemia, leukemia results in a highly cellular marrow and it consists of leukemic cells (H&E, X 400). c) Section from spleen tissue of AML showing shows marked hyperplasia (H&E, X 400).

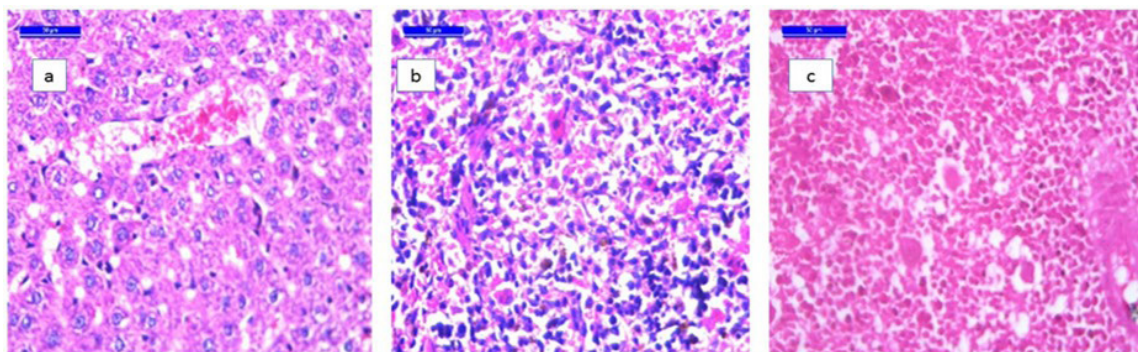


Figure 12. a) Section from liver tissue of AML + MNPs group showing moderate portal lymphocytic infiltrate, moderate ballooning degeneration (H&E, X 400). b) Section from bone marrow tissue of AML + MNPs showing Haematopoietically Active Bone Marrow Connective tissue stroma, Hematopoietic cords, Sinusoids (H&E, X 400). c) Section from spleen tissue of AML+ MNPs showing shows moderate hyperplasia (H&E, X 400).

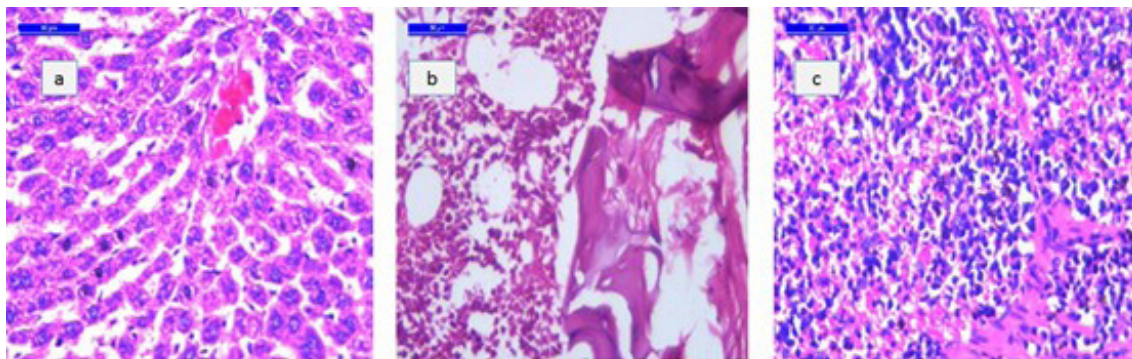


Figure 13. a) Section from liver tissue of AML +MFCS showing mild portal lymphocytic infiltrate, mild ballooning degeneration (H&E, X 400). b) Section from bone marrow tissue of AML+ MFCS showing Hematopoietic elements in this bone marrow biopsy is markedly reduced (H&E, X 400). c) Section from spleen tissue of AML + MFCS showing shows mild hyperplasia (H&E, X 400).

necrosis of liver tissue, aplastic anemia, and leukemic cells in bone marrow tissue with hyperplasia of spleen tissue compared to the normal appearance of control group Figure 10. Treatment of AML with MNPs caused moderate portal lymphocytic infiltrate with ballooning degeneration of liver, hematopoietically active bone marrow connective tissue stroma, hematopoietic cords, sinusoids of bone marrow with moderate hyperplasia of the spleen (Figure 12). On the other hand, treatment of AML with MFCS caused more significant improvement indicated by mild portal lymphocytic infiltrate and mild ballooning degeneration of liver tissue. Hematopoietic elements in this bone marrow biopsy are markedly reduced with mild hyperplasia of the spleen (Figure 13).

4. Conclusions

In conclusion, the results of *invitro* study could speculate that MNPs and FMCS have a cytotoxic and apoptotic effects that cause downregulation of Bcl-2 and upregulation of Caspase-3 expression. The use of the rat model signifies the correlation with the human system and suggests that exposure to nanosized particles causes adverse changes in animal biochemical and histological profiles. FMCS promotes apoptosis in part by enhancing Bcl-2 promoter methylation. These Bcl-2 promoter methylation responses, measured *invivo*, contribute to understanding the mechanisms involved in the amelioration of AML that was clear in FMCS treated group more than MNPs group. As controlling the expression of CD34 and CD38 by MFCS and MNPs, the expression of Bcl-2 proto-oncogene could be controlled and mitigate the progression of AML through regulating other parameters as β 2M. These findings contribute to our understanding of the mechanisms whereby folate NPs are effective against cancer especially leukemia. MFCS nanoparticles combine the two mechanisms and traits of magnetite and folate NPs with their multiple activities. The current study concluded that MFCS nanoparticles could be an implication for therapies that are geared towards inhibiting Bcl-2 gene expression and inducing apoptosis.

References

- AKBARZADEH, F., KHOSHGARD, K., ARKAN, E., HOSSEINZADEH, L. and AZANDARYANI, A.H., 2018. Evaluating the photodynamic therapy efficacy using 5-aminolevulinic acid and folic acid conjugated bismuth oxide nanoparticles on human nasopharyngeal carcinoma cell line. *Artificial Cells, Nanomedicine, and Biotechnology*, vol. 46, no. 3, pp. S514-S523. <http://dx.doi.org/10.1080/21691401.2018.1501376>.
- AL-SAADON, E.A., AL-NAAMA, L.M. and HASSAN, J.K., 2003. Serum lactate dehydrogenase (LDH) activity in children with malignant diseases. *Bahrain Medical Bulletin*, vol. 25, pp. 71-73.
- BARHAM, D. and TRINDER, P., 1972. Enzymatic colorimetric method for uric acid analysis. *Analyst (London)*, vol. 97, pp. 142. <http://dx.doi.org/10.1039/an9729700142>.
- CHANG, F., SHAMSI, T.S. and WARYAH, A.M., 2016. Clinical and hematological profile of acute Myeloid Leukemia (AML) Patients of Sindh. *Journal of Hematology & Thromboembolic Diseases*, vol. 4, no. 2, pp. 1-5.
- CHANG, Y., HSU, J., LIN, W., LEE, Y. and WANG, C., 2012. High incidence of acute promyelocytic leukemia specifically induced by N-nitroso-N-methylurea (NMU) in Sprague-Dawley rats. *Archives of Toxicology*, vol. 86, no. 2, pp. 315-327. <http://dx.doi.org/10.1007/s00204-011-0753-7>. PMID:21964634.
- CHIANG, K., TSUI, K., CHUNG, L., YEH, C., FENG, T., CHEN, W., CHANG, P., CHIANG, H. and JUANG, H., 2014. Cisplatin modulates B-cell translocation gene 2 to attenuate cell proliferation of prostate carcinoma cells in both p53- dependent and p53-independent pathways. *Scientific Reports*, vol. 4, no. 1, pp. 5511. <http://dx.doi.org/10.1038/srep05511>. PMID:24981574.
- CHO, Y., TURNER, N.D., DAVIDSON, L.A., CHAPKIN, R.S., CARROLL, R.J. and LUPTON, J.R., 2012. A chemoprotective fish oil/pectin diet enhances apoptosis via Bcl-2 promoter methylation in rat azoxymethane-induced Carcinomas. *Experimental Biology and Medicine (Maywood, N.J.)*, vol. 237, no. 12, pp. 1387-1393. <http://dx.doi.org/10.1258/ebm.2012.012244>. PMID:23354397.
- CIVIN, C.I., STRAUSS, L.C., BROVALL, C., FACKLER, M.J., SCHWARTZ, J.F. and SHAPER, J.H., 1984. Antigenic analysis of hematopoiesis. III. A hematopoietic progenitor cell surface antigen defined by a monoclonal antibody raised against KG-1a cells. *Journal of Immunology (Baltimore, Md.: 1950)*, vol. 133, no. 1, pp. 157-165. PMID:6586833.

- CONG, G., JIA, S., LUO, C. and WANG, Y., 2012. Folic acid prevents Bcl-2 hypomethylation in rats with hyperhomocysteinemia. *Wei Sheng Yen Chiu*, vol. 41, no. 2, pp. 268-272. PMID:22611939.
- DOKWAL, S., GHALAUT, V.S., LOKANATHAN, V., BANSAL, P., SARKAR, M. and GUPTA, G., 2016. Beta 2 Microglobulin (B2M) as a marker of disease severity and progression in acute myeloid leukemia (AML). *Scholars Academic Journal of Biosciences*, vol. 4, no. 7, pp. 589-594. <http://dx.doi.org/10.21276/sajb.2016.4.7.7>.
- ELSAVED, H.H., AL-SHERBINI, A.A.M., ABD-ELHADY, E.E. and AHMED, K.A., 2014. Treatment of anemia progression via magnetite and folate nanoparticles In Vivo. *ISRN Nanotechnology*, pp. 1-13. <http://dx.doi.org/10.1155/2014/287575>.
- FANG, X., WU, X., LI, C., ZHOU, B., CHEN, X., CHEN, T. and YANG, F., 2017. Targeting selenium nanoparticles combined with baicalin to treat HBV-infected liver cancer. *RSC Advances*, vol. 7, no. 14, pp. 8178-8185. <http://dx.doi.org/10.1039/C6RA28229F>.
- FIKRY, W.M.E., 2017. Lactate dehydrogenase (LDH) as prognostic marker in acute leukemia "Quantitative method". *Journal of Blood Disorders & Transfusion*, vol. 8, pp. 375. <http://dx.doi.org/10.4172/2155-9864.1000375>.
- GHOSH, S., SHINDE, S.C., KUMARAN, G.S., SAPRE, R.S., DHOND, S.R., BADRINATH, Y., ANSARI, R., KUMAR, A., MAHADIK, S., CHOUGULE, A.B. and NAIR, C.N., 2003. Hematologic and immunophenotypic profile of acute myeloid leukemia: an experience of Tata Memorial Hospital. *Indian Journal of Cancer*, vol. 40, no. 2, pp. 71-76. PMID:14716122.
- HAFIZ, M.D.G. and MANNAN, M.A., 2007. Serum lactate dehydrogenase level in childhood acute lymphoblastic leukemia. *Bangladesh Medical Research Council Bulletin*, vol. 33, no. 3, pp. 8-91. <http://dx.doi.org/10.3329/bmrcb.v33i3.1139>. PMID:18783063.
- HAFIZ, M.G. and ISLAM, A., 2009. Extensive skeletal lesions in childhood acute lymphoblastic leukemia. *Mymensingh Medical Journal*, vol. 18, no. 1, pp. 88-94. PMID:19182758.
- HASHEMIAN, A.R. and MANSOORI, G.A., 2013. Cancer nanodiagnostics and nanotherapeutics through the folate- conjugated nanoparticles. *Journal of Bioanalysis & Biomedicine*, vol. 5, no. 3, pp. 61-64. <http://dx.doi.org/10.4172/1948-593X.1000080>.
- HILL, B.T. and SEKERES, M.A., 2009. Acute Myeloid Leukemia. *Hematology*, vol. 3, no. 4, pp. 1-11. PMID:27414083.
- HWANG, S.M., 2020. Classification of acute myeloid leukemia. *The Korean Journal of Hematology*, vol. 55, no. S1, pp. S1-S4. <http://dx.doi.org/10.5045/br.2020.S001>. PMID:32719169.
- IBRAHIM, S., KEATING, M., DO, K.A., O'BRIEN, S., HUH, Y.O., JILANI, I., LERNER, S., KANTARJIAN, H.M. and ALBITAR, M., 2001. CD38 expression as an important prognostic factor in B-cell chronic lymphocytic leukemia. *Blood Research*, vol. 98, no. 1, pp. 181-186. <http://dx.doi.org/10.1182/blood.V98.1.181>. PMID:11418478.
- ISMAIL, S., MOHAMED, G., AMER, A. and AMER, M., 2020. Comparative killing activity of different nanoparticles and nanocomposites based on dermanyssusgallinae. *Nano Biomedicine and Engineering*, vol. 12, no. 4, pp. 338-350. <http://dx.doi.org/10.5101/nbe.v12i4.p338-350>.
- JARAHIAN, A., FATAHIAN, S. and SHAHANIPOUR, K., 2018. Investigation the effect of Fe3O4 nanoparticles on liver and stress oxidative parameters at the presence of magnetic field in rat. *Nanomedicine Journal*, vol. 5, no. 2, pp. 96-101. <http://dx.doi.org/10.22038/nmj.2018.005.006>.
- JENNINGS, C.D. and FOON, K.A., 1997. Recent advances in flow cytometry: application to the diagnosis of hematologic malignancy. *Blood*, vol. 90, no. 8, pp. 2863-2892. <http://dx.doi.org/10.1182/blood.V90.8.2863>.
- JIANG, Z., WU, D., LIN, S. and LI, P., 2016. CD34 and CD38 are prognostic biomarkers for acute B lymphoblastic leukemia. *Biomarker Research*, vol. 4, no. 1, pp. 1-4. <http://dx.doi.org/10.1186/s40364-016-0080-5>. PMID:28018598.
- JING, W., YI-JUE, C., PING, G. and QT-HUA, F., 2011. Changes of trace elements and nutritional proteins in children with acute leukemia at remission stage. *Chinese Journal of Clinical Nutrition*, vol. 19, pp. 84-87.
- JOSHI, D.M., KARODE, H.A. and SURALKAR, S.R., 2013. White blood cells segmentation and classification to detect acute leukemia. *International Journal of Emerging Trends & Technology in Computer Science*, vol. 2, no. 3, pp. 147-151.
- KUMARI, M., 2020. *Cancer notes. Unit 1. Nutrition in cancer*. Noida: Therapeutic Nutrition Amity Institute of Food Technology, AMITY University, pp. 1-15.
- KUMARI, M., RAJAK, S., SINGH, S.P., MURTY, U.S.P., MAHBOOB, M., GROVER, P. and RAHMAN, M.F., 2013. Biochemical alterations induced by acute oral doses of iron oxide nanoparticles in Wistar rats. *Drug and Chemical Toxicology*, vol. 36, no. 3, pp. 296-305. <http://dx.doi.org/10.3109/01480545.2012.720988>. PMID:23025823.
- LEVESQUE, R., 2007. *SPSS programming and data management: a guide for SPSS and SAS users*. 3rd ed. Chicago: SPSS Inc.
- LIU, Z., JIN, X., PI, W. and LIU, S., 2017. Folic acid inhibits nasopharyngeal cancer cell proliferation and invasion via activation of FRα/ERK1/2/ TSLC1 pathway. *Bioscience Reports*, vol. 37, no. 6, pp. BSR20170772. <http://dx.doi.org/10.1042/BSR20170772>. PMID:29070520.
- LIU, Z., ZHAO, J., CHEN, X.F., LI, W., LIU, R., LEI, Z., LIU, X., PENG, X., XU, K., CHEN, J., LIU, H., ZHOU, Q.H. and ZHANG, H.T., 2008. CpG island methylator phenotype involving tumor suppressor genes located on chromosome 3p in non-small cell lung cancer. *Lung Cancer (Amsterdam, Netherlands)*, vol. 62, no. 1, pp. 15-22. <http://dx.doi.org/10.1016/j.lungcan.2008.02.005>. PMID:18358560.
- LOW, P.S., HENNE, W.A. and DOORNEWEERD, D.D., 2008. Discovery and development of folic-acid based receptor targeting for imaging and therapy of cancer and inflammatory diseases. *Accounts of Chemical Research*, vol. 41, no. 1, pp. 120-129. <http://dx.doi.org/10.1021/ar7000815>. PMID:17655275.
- MATHEWS, E., LAURIE, T., O'RIORDAN, K. and NABHAN, C., 2008. Liver Involvement with Acute Myeloid Leukemia. *Case Reports in Gastroenterology*, vol. 2, no. 1, pp. 121-124. <http://dx.doi.org/10.1159/000120756>. PMID:21490850.
- MATSUEDA, K., YAMAMOTO, H. and DOI, I., 1998. An autopsy case of granulitic sarcoma of the porta hepatis causing obstructive jaundice. *Journal of Gastroenterology*, vol. 33, no. 3, pp. 428-433. <http://dx.doi.org/10.1007/s005350050108>. PMID:9658326.
- MONDAL, S., ADHIKARI, A., DAS, M., DARBAR, S., ALHARBI, A., AHMED, S.A., BHATTACHARYA, S.S., PAL, D. and PAL, S.K., 2019. Novel one pot synthesis and spectroscopic characterization of a folate-Mn3O4 nanohybrid for potential photodynamic therapeutic application. *RSC Advances*, vol. 9, no. 52, pp. 30216-30225. <http://dx.doi.org/10.1039/C9RA06835J>.
- MOSS, D.W., HENDERSON, A.R. and KACHMAR, J.F., 1987. Enzymes. In: N.W. TIETZ, ed. *Fundamentals of clinical chemistry*. 3rd ed. Philadelphia: WB Saunders, pp. 346-421.
- MUKHERJEE, S., LIANG, L. and VEISEH, O., 2020. Recent advancements of magnetic nanomaterials in cancer therapy. *Pharmaceutics*, vol. 12, no. 2, pp. 147. <http://dx.doi.org/10.3390/pharmaceutics12020147>. PMID:32053995.
- NAMVAR, F., RAHMAN, H.S., MOHAMAD, R., BAHARARA, J., MAHDAVI, M., AMINI, E., CHARTRAND, M.S. and YEAP, S.K., 2014. Cytotoxic effect of magnetic iron oxide nanoparticles synthesized via

- seaweed aqueous extract. *International Journal of Nanomedicine*, vol. 9, pp. 2479-2488. <http://dx.doi.org/10.2147/IJN.S59661>. PMID:24899805.
- NOVOTNA, B., JENDELOVA, P., KAPCALOVA JUNIOR, M., ROSSNER JUNIOR, P., TURNOVCOVA, K., BAGRYANTSEVA, Y., BABIC, M., HORAK, D. and SYKOVA, E., 2012. Oxidative damage to biological macromolecules in human bone marrow mesenchymal stromal cells labeled with various types of iron oxide nanoparticles. *Toxicology Letters*, vol. 210, no. 1, pp. 53-63. <http://dx.doi.org/10.1016/j.toxlet.2012.01.008>. PMID:22269213.
- OMSTEAD, D.T., MEJIA, F., SJOERDSMA, J., KIM, B., SHIN, J., KHAN, S., WU, J., KIZILTEPE, T., LITTLEPAGE, L.E. and BILGICER, B., 2020. In vivo evaluation of CD38 and CD138 as targets for nanoparticle-based drug delivery in multiple myeloma. *Journal of Hematology & Oncology*, vol. 13, no. 1, pp. 145-160. <http://dx.doi.org/10.1186/s13045-020-00965-4>. PMID:33138841.
- ORCIANI, M., TRUBIANI, O., GUARNIERI, S., FERRERO, E. and DIPRIMIO, R., 2008. CD38 is constitutively expressed in the nucleus of human hematopoietic cells. *Journal of Cellular Biochemistry*, vol. 105, no. 3, pp. 905-912. <http://dx.doi.org/10.1002/jcb.21887>. PMID:18759251.
- PENG, M.X., WANG, X.Y., WANG, F., WANG, L., XU, P.-P. and CHEN, B., 2016. Apoptotic mechanism of human leukemia K562/A02 cells induced by magnetic ferroferric oxide nanoparticles loaded with wogonin. *Chinese Medical Journal*, vol. 129, no. 24, pp. 2958-2966. <http://dx.doi.org/10.4103/0366-6999.195466>. PMID:27958228.
- PRIZMENT, A.E., LINABERY, A.M., LUTSEY, P.L., SELVIN, E., NELSON, H.H., FOLSOM, A.R., CHURCH, T.R., DRAKE, C.G., PLATZ, E.A. and JOSHU, C., 2017. Circulating beta-2 microglobulin and risk of cancer: the Atherosclerosis Risk in Communities Study (ARIC). *Cancer Epidemiology, Biomarkers & Prevention*, vol. 25, no. 4, pp. 657-664. <http://dx.doi.org/10.1158/1055-9965.EPI-15-0849>. PMID:26908438.
- REITMAN, S. and FRANKEL, S., 1957. A colorimetric method for the determination of serum glutamic oxaloacetic and glutamic pyruvic transaminases. *American Journal of Clinical Pathology*, vol. 28, no. 1, pp. 56-63. <http://dx.doi.org/10.1093/ajcp/28.1.56>. PMID:13458125.
- REVIA, R.A. and ZHANG, M., 2016. Magnetite nanoparticles for cancer diagnosis, treatment, and treatment monitoring: recent advances. *Materials Today*, vol. 19, no. 3, pp. 157-168. <http://dx.doi.org/10.1016/j.mattod.2015.08.022>. PMID:27524934.
- RUIZ, A., GUTIÉRREZ, L., CÁCERES-VÉLEZ, P.R., SANTOS, D., CHAVES, S.B., FASCINELLI, M.L., GARCIA, M.P., AZEVEDO, R.B. and MORALES, M.P., 2015. Biotransformation of magnetic nanoparticles as a function of the coating in a rat model. *Nanoscale*, vol. 7, no. 39, pp. 1-3. <http://dx.doi.org/10.1039/C5NR03780H>.
- SHEN, X., GE, Z. and PANG, Y., 2015. Conjugating folate on superparamagnetic Fe₃O₄@Aunanoparticles using click chemistry. *Journal of Solid State Chemistry*, vol. 222, pp. 37-43. <http://dx.doi.org/10.1016/j.jssc.2014.10.031>.
- SHIRBAND, A., AZIZIAN, H., POURENTEZARI, M., REZVANI, M.E., ANVARI, M., and ESMAEILDEHAJ, M., 2014. Dose-dependent effects of iron oxide nanoparticles on thyroid hormone concentrations in liver enzymes: possible tissue destruction. *Global Journal of Medicine Researches and Studies*, vol. 1, no. 1, pp. 28-31.
- SMITH, M., BARNETT, M., BASSAN, R., GATTA, G., TONDINI, C. and KERN, W., 2004. Adult acute myeloid leukaemia. *Critical Reviews in Oncology/Hematology*, vol. 50, no. 3, pp. 197-222. <http://dx.doi.org/10.1016/j.critrevonc.2003.11.002>. PMID:15182826.
- TORELLI, G.F., CASCINO, A., MUSCARITOLI, M., RUSSO, M., FALCONE, C., CHERUBINI, S. and FANELLI, F.R., 1997. Energy metabolism in cancer patients. *Minerva Gastroenterologica e Dietologica*, vol. 43, no. 4, pp. 183-188. PMID: 16501445.
- TSIMBERIDOU, A.M., KANTARJIAN, H.M., WEN, S., O'BRIEN, S., CORTES, J., WIERDA, W.G., KOLLER, C., PIERCE, S., BRANDT, M., FREIREICH, E.J., KEATING, M.J. and ESTEY, E.H., 2008. The prognostic significance of serum β 2 microglobulin levels in acute myeloid leukemia and prognostic scores predicting survival: analysis of 1,180 patients. *Clinical Cancer Research*, vol. 14, no. 3, pp. 721-730. <http://dx.doi.org/10.1158/1078-0432.CCR-07-2063>. PMID:18245532.
- TYAGI, S., RAWAT, S. and SAXENA, S., 2016. Folate conjugates: a boon in the anti-cancer therapeutics. *IJPSR*, vol. 7, no. 11, pp. 4278-4303. [http://dx.doi.org/10.13040/IJPSR.0975-8232.7\(11\).4278-03](http://dx.doi.org/10.13040/IJPSR.0975-8232.7(11).4278-03).
- VIEIRA, M.N.N., FIGUEROA-VILLAR, J.D., MEIRELLES, M.N.L., FERREIRA, S.T. and DE FELICE, F.G., 2006. Small molecule inhibitors of lysozyme amyloid aggregation. *Cell Biochemistry and Biophysics*, vol. 44, no. 3, pp. 549-553. <http://dx.doi.org/10.1385/CBB:44:3:549>. PMID:16679543.
- WANG, F., LV, H., ZHAO, B., ZHOU, L., WANG, S., LUO, J., LIU, J. and SHANG, P., 2019. Iron and leukemia: new insights for future treatments. *Journal of Experimental & Clinical Cancer Research*, vol. 38, no. 1, pp. 406. <http://dx.doi.org/10.1186/s13046-019-1397-3>. PMID:31519186.
- WANG, M.S., CHEN, L., XIONG, Y.Q., XU, J., WANG, J.P. and MENG, Z.L., 2017. Iron oxide magnetic nanoparticles combined with actein suppress non-small-cell lung cancer growth in a p53-dependent manner. *International Journal of Nanomedicine*, vol. 12, pp. 7627-7651. <http://dx.doi.org/10.2147/IJN.S127549>. PMID:29089760.
- YAMAUCHI, T., NEGORO, E., LEE, S., TAKAI, M., MATSUDA, Y., TAKAGI, K., KISHI, S., TAI, K., HOSONO, N., TASAKI, T., IKEGAYA, S., INAI, K., YOSHIDA, A., URASAKI, Y., IWASAKI, H., and UEDA, T., 2013. A high serum uric acid level is associated with poor prognosis in patients with acute myeloid leukemia. *Anticancer Research*, vol. 33, pp. 3947-3952. PMID: 24023333.
- YU, Q., XIONG, X., ZHAO, L., XU, T., BI, H., FU, R. and WANG, Q., 2018. Biodistribution and toxicity assessment of superparamagnetic iron oxide nanoparticles in vitro and in vivo. *Current Medical Science*, vol. 38, no. 6, pp. 1096-1102. <http://dx.doi.org/10.1007/s11596-018-1989-8>. PMID:30536075.